Slow Earthquakes: A Manifestation of Transitional Frictional Behavior

J.R. Leeman, D.M. Saffer, C. Marone

1 Introduction

Observations of slow-slip and low-frequency earthquakes in nature suggest that fault failure encompasses a spectrum of slip modes [1, 2, 3]. While the explanations for non-traditional earthquakes remain a topic of debate, they have been observed in many subduction zones, including Cascadia [4, 5], Mexico [6], Costa Rica [7], Japan [8], and New Zealand [9]. What causes strain energy to be released across a wide-range of failure behaviors is not well understood, but transitional frictional stability is a possible explanation. System stability is defined in terms of system stiffness (k) related to the critical stiffness (k_c) [10] and can be altered by environmental variables such as effective normal stress, critical slip distance, and the velocity dependence of friction. Clustering of slow and transitional events around traditional seismic faults in nature suggests that transitional behavior is responsible. Laboratory evidence of this behavior is scattered [11, 12, 13], mostly suggested by numerical models [10]. Here we present the first systematic investigation of the critical stiffness ratio and its effect on the frictional state of a laboratory fault. We also show that stiffness can control the slip mode and that the slip mode can change as stiffness is influenced by accumulated fault slip and damage zone evolution.

2 Main

The observation of non-traditional slip modes (slow slip, very low frequency earthquakes, episodic tremor and slip, etc) in a wide variety of locations over the last decade suggests that this is a common occurrence. There have been suggestions that these behaviors, often observed at the down-dip limit of traditional seismic slip, can influence, interact with, or trigger up-dip earthquakes [14, 15]. There has also been the suggestion that these events occur at the transition between stable and locked patches of a fault and that non-traditional slip areas could influence earthquake nucleation in those areas [16].

The rate-and-state friction framework is commonly used to describe the dynamic frictional behavior of natural and experimental systems to perturbations. This empirical relation consists of the parameters a and b which describe the velocity dependence of friction. For materials in which $(a-b) > 0$ the friction increases with increased driving velocity, termed velocity strengthening. Likewise, materials with $(a-b) < 0$ are velocity weakening. The model also consists of an e-folding critical slip distance D_c, and a state variable θ. D_c is thought of, in the laboratory, as the distance required to completely renew a contact population. The state variable is thought to be a proxy for

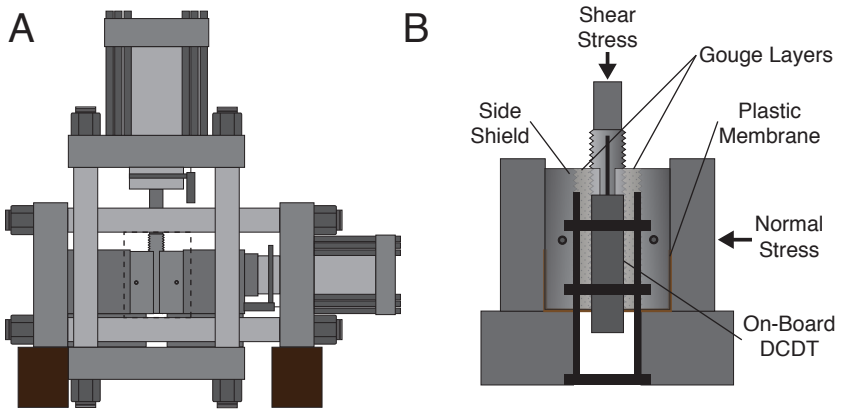

Figure 1: The biaxial deformation apparatus (A) and sample configuration (B). Two large hydraulic pistons are servo-controlled in either force or displacement control modes. Double direct shear samples are supported by steel blocks. Samples use metal side shields and a plastic membrane to reduce gouge extrusion. Local displacement transducers (DCDTs) can be referenced to the center block to avoid apparatus stiffness effects on the measurement.

the age of the frictional contacts, and evolves according to a state evolution relation, commonly the Dieterich 'slowness' or Runia 'slip' relation [17, 18, 19].

For unstable behavior to occur: 1) that the material be velocity neutral to velocity weakening, and 2) that the system stiffness be at or below the critical stiffness [17, 20]. If a material is velocity strengthening, any acceleration leading to slip is immediately arrested by increased shearing resistance and the energy is frictionally dissipated. The stiffness of the system governs the rate at which energy stored as strain can be released. If the energy release occurs in such a way that the drop in shear resistance with displacement occurs faster than the drop in applied shearing force with displacement, the system can support unstable failure. The critical stiffness can be described in terms of the rate-and-state parameters as (eq.1). The aggregate stiffness of the loading system and sample can be measured by fitting the linear-slope of the load-point displacement vs. shear load curve on either an unload/reload cycle or on the loading portion of a single stick-slip event [13].

$$K_c = \sigma_n' \frac{b-a}{D_c} \tag{1}$$

We conducted a suite of biaxial double-direct shearing experiments with a fine quartz fault gouge simulant (Min-U-Sil®), chosen for its geologic relevance, reproducible results, and well controlled composition and size distribution. This study systematically examines the behavior of an experimental fault as a function of nearness to the stability criterion $k \sim k_c$. Using the same, well controlled sample material for each experiment and humidifying the samples, we ensure that the rate-and-state parameters (a, b, D_c) remain essentially constant between experiments. We then explore the stability of the system by modifying the stiffness directly by changing the forcing block configuration and by changing the applied effective normal stress (σ_n').

In order to define/measure the RSF parameters for each experiment, we use a range of measurements. For experiments in which K is high, stable sliding behavior is observed and we use velocity steps to obtain the rate-and-state frictional parameters and therefore K_c. We assume that the

evolution of these material and layer properties is not dependent on the mode of slip, and therefore we use the values measured on stably sliding experiments as a framework for evaluating/comparing results from the suite of experiments.

3 Results/Discussion

Our results show that the mode of slip is consistent with that expected from the rate-and-state friction framework. Slip mode varies systematically with K, and transitional behavior is observed at $\frac{K}{K_c} \sim 1$. In a stiff (all steel) forcing setup, linearly stable behavior was observed, while in a more compliant loading system, emergent unstable behavior was observed. Unstable behavior began with frictional oscillations, transitionally to dynamic frictional failure. Oscillations and dynamic failure are characterized by relatively rapid accelerations and decelerations of the system above/below the load point velocity when the material yields under excessive shear force. In experiments with further increased compliance, rapid dynamic failure was observed. These events were audible and classified as fast stick-slip.

We also observe that there is a relation between the peak velocity or duration of slip and $\frac{K}{K_c}$. Systems near the stability transition exhibit lower peak velocities and long duration events, seen as frictional oscillations in the experiments. The further the system is from the transition, the events become shorter in duration and faster.

Both K and K_c, and thus mode of slip, evolve with net slip. As layer accumulates strain and strain is localized, it stiffens. At the same time, RSF parameters evolve, modifying the critical stiffness of the system. This explains a rich variety of behaviors that may appear unrelated or non-linear initially. This is supported by our observations that stick slip does not occur until a critical displacement is reached, because K_c is negative until the onset of rate weakening behavior. Most stiffness evolution occurs in the first 10 mm of shear, asymptotically approaching stead-state. Initial increases in stiffness could be due to layer compaction from grain rearrangement, layer thinning with increased shear strain, grain comminution, localization of shear, or reduction of compliant center block material above the sample due to geometric effects. Layer compaction due to rearrangement and geometric thinning with shear have been well documented [21]. At these low stresses, grain comminution is minimal. Shear localization effects have been shown to play a role in the evolution of layer behavior [22], especially before reaching mechanical steady-state as R and Y shears develop. The reduction in the amount of compliant center block material above the shearing zone with accumulated displacement is minimal compared to these other effects.

In our experiments, a remains relatively constant with displacement, but b evolves asymptotically upwards with increasing shear displacement. During this transitional period, the critical slip distance evolves downwards (Fig.2).

Our results support previous ideas about the role of transitional frictional properties in supporting a range of complex failure behaviors. Natural factors such as compliant and evolving damage zones, low effective normal stress [23, 24, 25], and fault evolution/aging [26] are all captured in the simple ratio of $\frac{K}{K_c}$. All of this suggesting that tectonic faults may change behavior as they accumulate slip and become mature fault zones.

In nature, the critical patch size is thought of as the size a crack must grow to before being able to support propagating dynamic rupture. Shallow VLF events in Nankai have been shown to have critical patch sizes of $L_c = 37 - 63$ m, comparable to laboratory tests on natural materials from

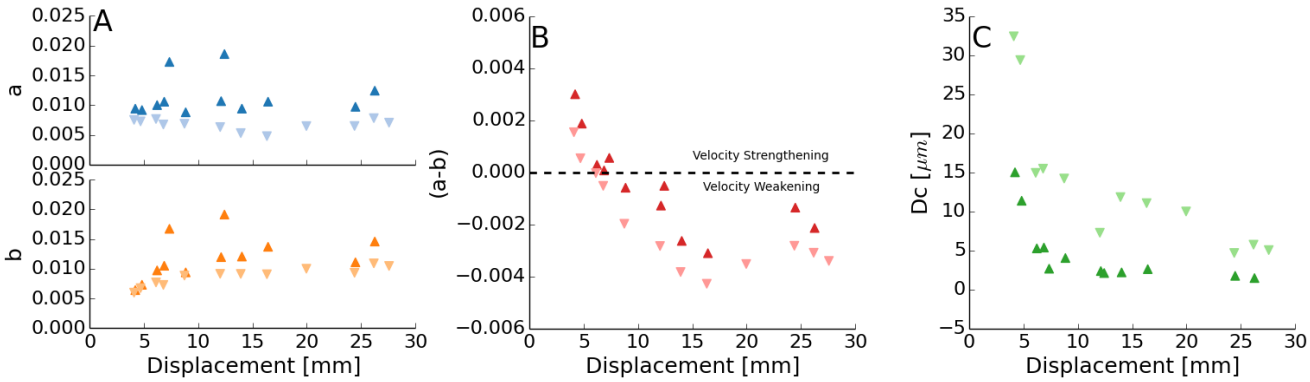

Figure 2: Rate-and-state friction parameters obtained from velocity step inversions. All inversions were accomplished with a fixed stiffness of k =5.5x10$^{-3}\mu$m. A) rate-and-state parameter a remains relatively constant with displacement and shows a systematic behavior with higher values of a always being observed during velocity up-steps. The b parameter shows a similar behavior, but also increases with displacement, reaching a steady-state value ∼10 mm displacement. B) The sample transitions from velocity strengthening to velocity weakening behavior at ∼10 mm and remains velocity weakening for the remainder of the experiment. C) Critical slip distance estimates show considerable scatter, but do reduce to a steady-state value of 5-10 um.

the area [27]. We likewise calculate patch sizes of 10's of meters for our experiments, but in a simple quartz gouge, not relying on slip dependent clay material properties. We would expect large critical patch sizes for environments with low effective normal stress (such as areas of high pore fluid pressure), small critical stiffness values, or reduced moduli.

$$r_c = \frac{16}{7\pi} G \frac{D_c}{\sigma_n (b-a)} \tag{2}$$

With slow-slip failure events, we see little to no dynamic overshoot. This is observable by a period of no block motion or deformation after the rapid stress-drop (Fig.3C). In traditional fast stick-slip events, the system shears further than required to complete the force balance. Frictional oscillations and slow-slip show no such overshoot, with continual deformation of the system throughout the simulated seismic cycle. This provides some insight into the low frequency nature of emissions observed from slow-slip and lack of audible report in the laboratory. Lower shear stiffnesses will reduce the seed of rupture propagation, softening step-like acceleration/deceleration pulses that result in high frequency emission. Slowed rupture velocities would also influence disaster potential, as tsunamogenic earthquake have generally slow rupture velocities [28, 29].

We suggest that where in the spectrum of failure behavior a fault lies can be quantitatively described by the relation of the stiffness of the fault compared to the calculated critical stiffness. While factors such as pore pressure and material frictional response are important, they are already factored into the stiffness comparison.

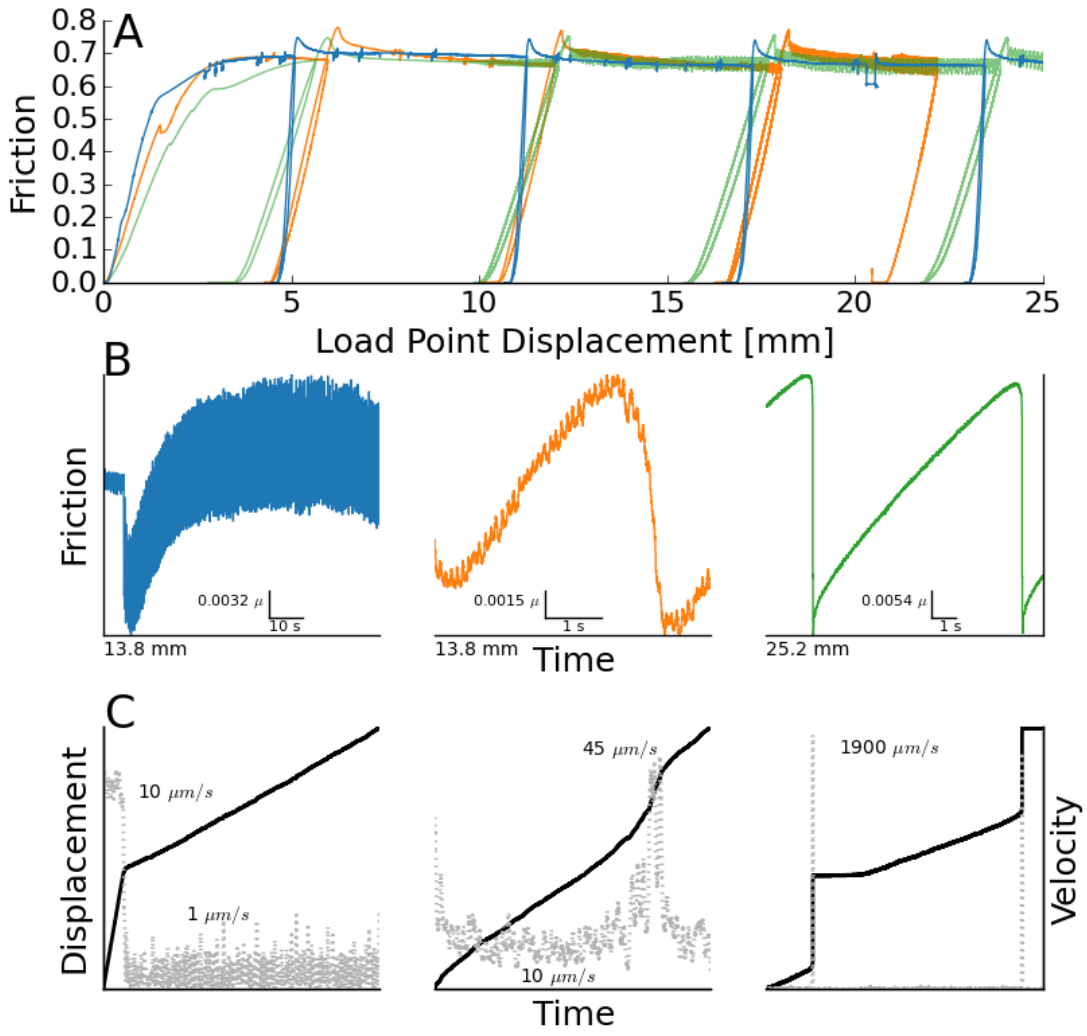

Figure 3: A) Run-plots of experiments p4309 (blue), p4311 (orange), and p4316 (green). Different working stiffnesses can be observed as the slope of unload/reload segments. B) All steel blocks produced stable responses to velocity steps (left). Destiffening the system with an acrylic center block produced non-audible slow-slip events (center). Further destiffening with an acrylic center block and increased normal stress produced audible fast stick-slip events(right). C) Center block displacement (black) and velocity (gray) for the corresponding types of failure.

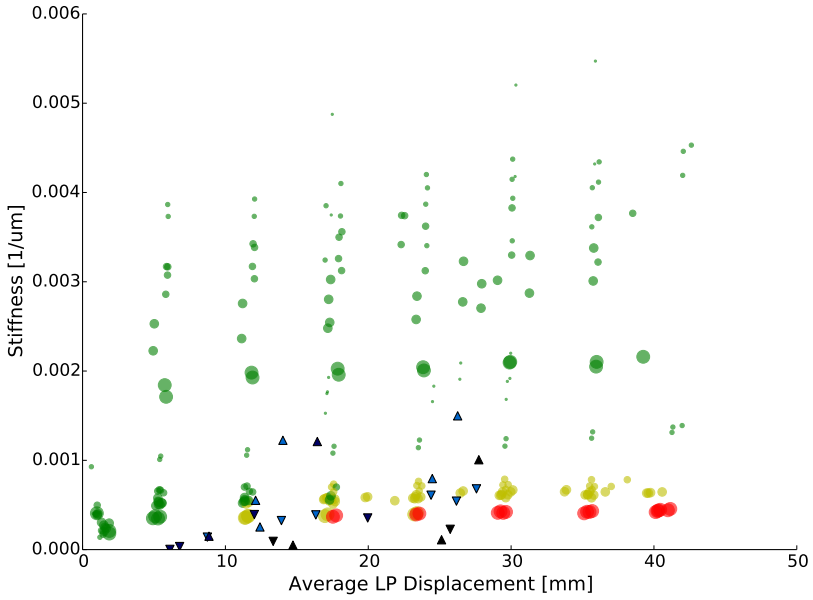

Figure 4: Stiffness estimates from shear stress unload/reload cycles show an increase in the stiffness early in shearing, likely associated with fabric development. Experiments with stiffness comparable to the critical stiffness estimates from velocity steps exhibit slow-slip behavior. Experiments in which the measured stiffness is below the critical stiffness exhibited more rapid, audible stick-slip.

4 Methods

All experiments were performed on a servo-controlled biaxial shearing apparatus. Displacements on the normal and shearing axes were measured by Direct Current Displacement Transducers (DCDTs) referenced at the end-platens and ram nose. The displacement of the shearing block was measured with a DCDT referenced at the end-platen and the top of the shearing block. Loads applied to the sample were measured with strain gauge load cells. All transducers are semi-annually calibrated with traceable transfer standards.

Samples were prepared in the double-direct-shear geometry using steel or titanium side blocks and steel or acrylic shearing blocks. All blocks were grooved 0.8 mm deep at 1 mm spacing to reduce boundary effects [30]. The sample area was 10 x 10 cm and filled with Min-U-Sil to a thickness of 3 mm. Granular layers were left in a sealed container overnight with a solution of anhydrous sodium carbonate to humidify the samples.

After samples were loaded into the load frame, a constant normal stress was applied and maintained by the servo system in a force feedback control mode. Samples were allowed to compact and accommodate grain rearrangement before shearing began. Shearing is conducted at a fixed rate in displacement feedback control mode.

Stiffness of the system was altered by changing the applied normal stress and by changing the material of the shearing block. Increasing normal stress decreases the effective stiffness of the system, as does switching the steel forcing block for a cast acrylic block.

Layers were built of Min-U-Sil® 40 fine ground silica from the U.S. Silica® company Berkeley Springs, West Virginia plant. The median diameter of grain is 10.5 μm. The product is 99.5 %

SiO_2, with traces of metal oxides making up the remainder.

System stiffnesses from unload/reload shear stress cycles were calculated by a least-squares linear fit in friction vs. displacement for the interval $\mu = 0.3 - 0.4$. Stiffnesses from the loading portion of slow-slip and stick-slip events were obtained with a derivative based algorithm [13]. Rate-and-state models were fit with both the Dieterich and Ruina laws, with comparable results. Inversions were done with an iterative singular value decomposition technique.

References

[1] Zhigang Peng and Joan Gomberg. An integrated perspective of the continuum between earthquakes and slow-slip phenomena. *Nature Geosci*, 3(9):599–607, 8 2010.

[2] Satoshi Ide, Gregory C. Beroza, David R. Shelly, and Takahiko Uchide. A scaling law for slow earthquakes. *Nature*, 447(7140):76–9, 5 2007.

[3] Gregory C. Beroza and Satoshi Ide. Slow earthquakes and nonvolcanic tremor. *Annual Review of Earth and Planetary Sciences*, 39(1):271–296, 5 2011.

[4] M. Meghan Miller, Tim Melbourne, Daniel J. Johnson, and William Q. Sumner. Periodic slow earthquakes from the cascadia subduction zone. *Science*, 295(5564):2423–2423, 2002.

[5] Garry Rogers and Herb Dragert. Episodic tremor and slip on the cascadia subduction zone: The chatter of silent slip. *Science*, 300(5627):1942–1943, 2003.

[6] Vladimir Kostoglodov. A large silent earthquake in the guerrero seismic gap, mexico. *Geophysical Research Letters*, 30(15), 2003.

[7] Yan Jiang, Shimon Wdowinski, Timothy H. Dixon, Matthias Hackl, Marino Protti, and Victor Gonzalez. Slow slip events in costa rica detected by continuous gps observations, 2002-2011. *Geochemistry, Geophysics, Geosystems*, 13(4), 4 2012.

[8] Yoshihiro Ito and Kazushige Obara. Very low frequency earthquakes within accretionary prisms are very low stress-drop earthquakes. *Geophysical Research Letters*, 33(9), 2006.

[9] Laura M. Wallace and John Beavan. Diverse slow slip behavior at the hikurangi subduction margin, new zealand. *J. Geophys. Res.*, 115(B12), 2010.

[10] Ji-Cheng Gu, James R Rice, Andy L Ruina, and Simon T Tse. Slip motion and stability of a single degree of freedom elastic system with rate and state dependent friction. *Journal of the Mechanics and Physics of Solids*, 32(3):167–196, 1984.

[11] Bryan M. Kaproth and C. Marone. Slow earthquakes, preseismic velocity changes, and the origin of slow frictional stick-slip. *Science*, 341(6151):1229–32, 9 2013.

[12] T. Baumberger, F. Heslot, and B. Perrin. Crossover from creep to inertial motion in friction dynamics. *Nature*, 367(6463):544–546, 1994.

[13] J.R. Leeman, M.M. Scuderi, C. Marone, and D.M. Saffer. Stiffness evolution of granular layers and the origin of repetitive, slow, stick-slip frictional sliding. *Granular Matter*, Submitted.

[14] H Dragert, K L Wang, and T S James. A silent slip event on the deeper Cascadia subduction interface. *Science*, 292(5521):1525–1528, 2001.

[15] Satoshi Ide, David R Shelly, and Gregory C Beroza. Mechanism of deep low frequency earthquakes: Further evidence that deep non-volcanic tremor is generated by shear slip on the plate interface. *Geophysical Research Letters*, 34(3):L03308, February 2007.

[16] A T Linde, M T Gladwin, MJS Johnston, R L Gwyther, and R G Bilham. A slow earthquake sequence on the San Andreas fault. *Nature*, 383(6595):65–68, 1996.

[17] Chris Marone. Laboratory-derived friction laws and their application to seismic faulting. *Annual Review of Earth and Planetary Sciences*, 26(1):643–696, 1998.

[18] James H. Dieterich. Modeling of rock friction: 1. experimental results and constitutive equations. *Journal of Geophysical Research: Solid Earth (1978–2012)*, 84(B5):2161–2168, 1979.

[19] Andy Ruina. Slip instability and state variable friction laws. *Journal of Geophysical Research: Solid Earth (1978–2012)*, 88(B12):10359–10370, 1983.

[20] Christopher H. Scholz. *The mechanics of earthquakes and faulting*. Cambridge University Press, 2002.

[21] David R. Scott, Chris J. Marone, and Charles G. Sammis. The apparent friction of granular fault gouge in sheared layers. *Journal of Geophysical Research: Solid Earth*, 99(B4):7231–7246, 1994.

[22] J. M. Logan, C. A. Dengo, N. G. Higgs, and Z. Z. Wang. Fabrics of experimental fault zones: Their development and relationship to mechanical behavior. *International Geophysics*, 51:33–67, 1992.

[23] Pascal Audet, Michael G Bostock, Nikolas I Christensen, and Simon M Peacock. Seismic evidence for overpressured subducted oceanic crust and megathrust fault sealing. *Nature*, 457(7225):76–78, 2009.

[24] Hiroko Kitajima and Demian M Saffer. Elevated pore pressure and anomalously low stress in regions of low frequency earthquakes along the nankai trough subduction megathrust. *Geophysical Research Letters*, 39(23), 2012.

[25] David R Shelly. Complexity of the deep san andreas fault zone defined by cascading tremor. *Nature Geoscience*, 2015.

[26] Matt J Ikari, Chris Marone, and Demian M Saffer. On the relation between fault strength and frictional stability. *Geology*, 39(1):83–86, 2011.

[27] Matt J. Ikari, Chris Marone, Demian M. Saffer, and Achim J. Kopf. Slip weakening as a mechanism for slow earthquakes. *Nature Geosci*, 6(6):468–472, 5 2013.

[28] Hiroo Kanamori and Masayuki Kikuchi. The 1992 nicaragua earthquake: a slow tsunami earthquake associated with subducted sediments. *Nature*, 361(6414):714–716, 1993.

[29] Susan L. Bilek and Thorne Lay. Rigidity variations with depth along interplate megathrust faults in subduction zones. *Nature*, 400(6743):443–446, 1999.

[30] Jennifer L. Anthony and Chris Marone. Influence of particle characteristics on granular friction. *Journal of Geophysical Research: Solid Earth*, 110(B8), 2005.

5 Acknowledgements

The authors wish to thank Steve Swavely for his support in the laboratory. We also thank Marco Scuderi for many discussions regarding this work. This material is based upon work supported by the National Science Foundation under Grant No. DGE1255832. Any opinions, findings, and conclusions or recommendations expressed in this material are those of the author(s) and do not necessarily reflect the views of the National Science Foundation. The work was also supported by funds from the GDL Foundation and Shell Oil Company.

6 Author Contributions

All authors contributed to data interpretation, analysis schema, and writing. J. Leeman conducted experiments and data analysis.

7 Competing Financial Interests

The authors declare no competing financial interests. Supplementary information accompanies this paper on www.nature.com/naturegeoscience. Reprints and permissions information is available online at http://npg.nature.com/reprintsandpermissions. Correspondence and requests for materials should be addressed to J.R. Leeman.

8 Supplementary

Experiment	Blocks Used	Normal Stress [MPa]	Temperature [°C]	Relative Humidity [%]	Comments	Unload/Reloads
p4224	Titanium/Acrylic	5	26	16	Stable - Velocity Steps	N
p4228	Steel	4	24	100	Stable - Slide Hold Slide	N
p4229	Titanium/Acrylic	4	24	100	Failed Experiment	N
p4248	Titanium/Acrylic	4	24.2	100	Stable - Velocity Steps	N
p4249	Titanium/Acrylic	4	23.2	100	Stable - Velocity Steps	N
p4267	Titanium/Acrylic	2	23.2	100	Stable - Velocity Steps	Y
p4268	Titanium/Acrylic	8	23.4	100	Slow Slip	Y
p4269	Steel	4	23.4	100	Stable - Velocity Steps	Y
p4270	Steel	2		100	Stable - Velocity Steps	Y
p4271	Titanium/Acrylic	2		100	Stable - Velocity Steps	Y
p4272	Titanium/Acrylic	8	22.7	100	Slow Slip	Y
p4273	Steel	8	23.4	100	Stable - Velocity Steps	Y
p4309	Steel	8	23.2	100	Stable - Velocity Steps	Y
p4310	Titanium/Acrylic	8	24.2	100	Slow Slip	Y
p4311	Titanium/Acrylic	8	23.3	100	Slow Slip	Y
p4312	Steel/Acrylic	8	23.6	100	Slow Slip	Y
p4313	Titanium/Acrylic	8	23.5	100	Slow Slip	Y
p4314	Steel	12	24.3	100	Stable - Velocity Steps	Y
p4316	Titanium/Acrylic	12	23.6	100	Stick Slip	Y
p4317	Steel/Acrylic	12	24.2	100	Stick Slip	Y
p4327	Steel	6	22.5	100	Stable - Velocity Steps	Y
p4328	Titanium/Acrylic	6	22.7	100	Slow Slip	Y
p4329	Titanium/Acrylic	6	22	100	Slow Slip	Y
p4330	Steel	6	22.9	100	Stable - Velocity Steps	Y
p4338	Titanium/Acrylic	4	24.2	100	Stable - Velocity Steps	Y
p4339	Steel	4	24.8	100	Stable - Velocity Steps	Y
p4340	Titanium/Acrylic	8	24.0	100	Slow Slip	Y
p4341	Steel	12	23.4	100	Stable - Velocity Steps	Y
p4342	Titanium/Acrylic	12	24.3	100	Slow/Fast Slip	N
p4343	Steel/Acrylic	6	23.9	100	Slow Slip	N
p4344	Titanium/Acrylic	7	24.5	100	Slow Slip	N
p4345	Steel/Acrylic	8	24.2	100	Slow Slip	N
p4346	Titanium/Acrylic	9	24.2	100	Slow Slip	N
p4347	Steel/Acrylic	10	23.1	100	Slow/Fast Slip	N
p4348	Titanium/Acrylic	11	23.9	100	Slow/Fast Slip	N
p4350	Steel/Acrylic	13	22.7	100	Slow/Fast Slip	N
p4351	Titanium/Acrylic	14	23.1	100	Slow/Fast Slip	N

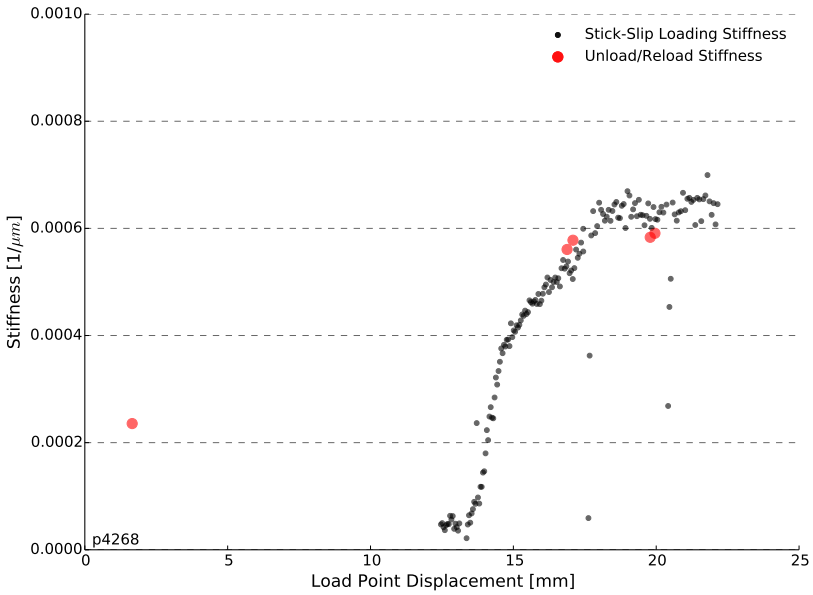

Figure 5: When the system is at steady-state, the two methods of stiffness estimation provide comparable results. At low displacements, early stick-slip events appear more compliant than bulk system measurements. This is due to the not fully dynamic failure of the events and creep during the loading phase.